ACS APPLIED MATERIALS & INTERFACES

www.acsami.org Research Article

# Facile In Situ Hydrothermal Synthesis of Layered Zirconium Phenylphosphonate Molecular Sieve Membranes with Optimized Microstructure and Superb $H_2/CO_2$ Selectivity

Taotao Ji, Yanwei Sun, Yi Liu, Mingrun Li, Fei Wang, Liangliang Liu, Gaohong He, and Yi Liu*

**Cite This:** *ACS Appl. Mater. Interfaces* 2020, 12, 15320−15327

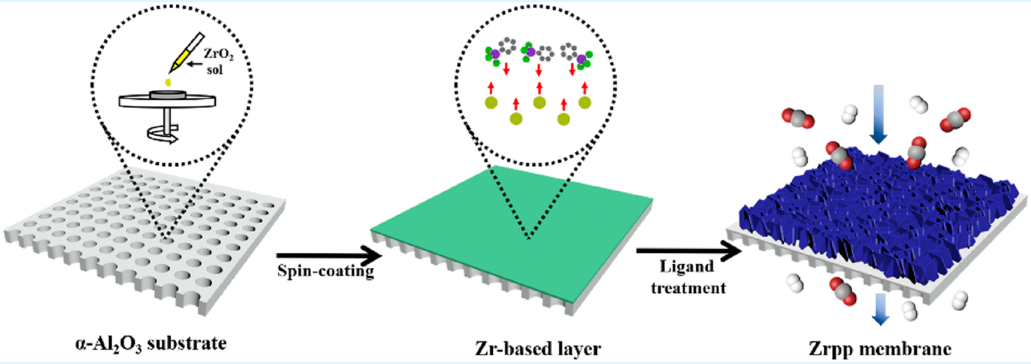

**ABSTRACT:** Layered molecular sieve membranes containing uniform interlayer galleries have offered unprecedented opportunities to reach a performance far beyond the Robeson upper bound line. In this study, we took the initiative to prepare layered zirconium phenylphosphonate (ZrPP) molecular sieve membranes with optimized microstructure on tetragonal zirconia ($t$-$ZrO_2$) buffer layer-modified porous $\alpha$-$Al_2O_3$ substrates by facile in situ hydrothermal growth. Relying on the 3.2 Å-sized gallery height and preferential $CO_2$ adsorption behavior, prepared ZrPP membranes showed exceptional $H_2/CO_2$ selectivity (>100) as well as considerable $H_2$ permeability. Furthermore, extraordinary thermal, mechanical, and chemical stability of ZrPP membranes made them potentially attractive for long-term operations under harsh conditions.

**KEYWORDS:** *membranes, zirconium phosphate, interlayer galleries, hydrothermal synthesis, cabron dioxide capture*

## 1. INTRODUCTION

Molecular sieve membranes including zeolite, metal−organic framework (MOF), silica, or carbon have shown unprecedented opportunities for energy-efficient gas separation in recent decades because of their very promising prospects for overcoming Robeson upper bound line.[1−6] In particular, development of new membrane materials with unique framework at the microscopic scale and optimized microstructure at the mesoscopic scale represents an effective approach for further performance enhancement of molecular sieve membranes. On one hand, deliberate design and reticular synthesis of membrane materials (such as MOF materials) enable fine-tuning of their pore aperture and functionality as in the case of propane-selective ZIF-8 membranes;[7−10] on the other hand, microstructure optimization (like preferred orientation control) benefits ordered arrangement of pores, decrease of grain boundary defects and reduction in diffusion barriers as is the case with $p$-xylene-selective $b$-oriented MFI zeolite membranes.[11−16] In addition, maintaining high thermal, chemical, and mechanical stability when applied in real operating conditions remains a great challenge for several molecular sieve membranes like 2D laminar membranes (such as graphene oxide, MXene, and transition-metal dichalcogenide) as these laminar layers are held by weak van der Waals force.[17−22] Last but not least, a facile synthetic method is preferred for large-scale membrane production.

Using a facile in situ hydrothermal growth method, we recently prepared NiAl-$CO_3$ layered double hydroxide (LDH) membranes exhibiting unprecedented $H_2/CH_4$ selectivity by relying on a uniform 3.2 Å-sized gallery height, which may be tuned by the intercalation of different charge compensating anions. Nevertheless, LDH-based membranes suffered from relatively lower $H_2$ permeability, owing to substantial charge compensating anions located in interlayer galleries, which may

**Received:** February 13, 2020
**Accepted:** March 11, 2020
**Published:** March 11, 2020

generate additional mass transfer barrier for fast diffusion of guest molecules. In addition, our membranes could not withstand operating temperature above 180 °C because of an irreversible collapse of the layered structure at this temperature.[23,24] Herein we try to develop new membrane materials to solve above-mentioned issues.

In recent decades, zirconium phosphate and its derivatives have been evaluated as ideal candidates for ion exchangers, catalysts, anticorrosion coatings, and drug delivery hosts.[25−29] Their potential as separation membranes, however, has not been explored yet. Because of the high Zr−O bond strength and high coordination number of Zr ions,[30−32] zirconium phosphate molecular sieve membranes may exhibit excellent thermal, chemical, and water stability, which is quite beneficial for their long-term operation under harsh conditions; moreover, the highly polarizing environment exhibits strong affinity for polarizable molecules like $CO_2$, which may result in a higher selectivity toward $CO_2$.[33] In addition, through incorporation of diverse phosphoric (phosphonic) acid ligands with different functional groups (e.g., hydroxyl, phenyl, etc.), both the gallery height and adsorption behavior of zirconium phosphate could be flexibly adjusted.[34]

Layered zirconium phenylphosphonate (ZrPP) as a representative of zirconium phosphate materials is formed by zirconium atoms coordinated by phenylphosphonate groups. Each phenylphosphonate contributes three oxygen atoms to the formation of these layers, leaving one benzene ring pointing into the interlayer space (shown in Figure S1).[35,36] ZrPP has been considered as promising candidates for $H_2$/$CO_2$ selective membranes due to an appropriate gallery height (3.2 Å) and strong affinity between $CO_2$ and highly polarized ZrPP framework. Moreover, compared with charged layered materials like ionic/anionic clays,[23,24,37] no charge compensating anions/ions existed within interlayer galleries so that diffusion barriers for guest molecules could be reduced.

In the present study, we took the initiative in facile in situ hydrothermal synthesis of well-intergrown ZrPP membranes by self-conversion of $t$-$ZrO_2$ buffer layer-modified porous $\alpha$-$Al_2O_3$ substrates in an aqueous solution containing phenylphosphonic acid ($C_6H_7O_3P$) and HF acid (experimental details were shown in Figure 1). With this method the formation of single-layer ZrPP nanosheets, their self-assembly into bulk ZrPP crystallites and firm attachment to porous $\alpha$-$Al_2O_3$ substrates could be accomplished in one step as demonstrated by microstructural evolution of ZrPP powders during hydrothermal growth (shown in Figure SI-2). As will be shown below, we noted that interlayer galleries of ZrPP membranes preferred to vertically aligned on substrates, which was very beneficial for their performance enhancement. In addition, ZrPP membranes were partially penetrated into the substrate pores, which was quite useful for improving their mechanical stability.

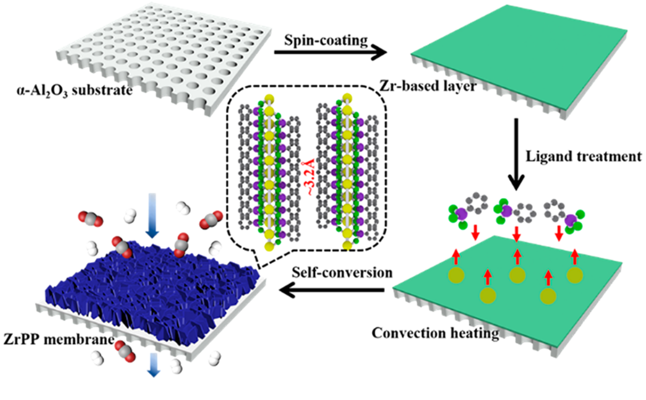

Figure 1. Schematic illustration of preparation of ZrPP membranes by hydrothermal conversion of $t$-$ZrO_2$ buffer layers.

## 2. EXPERIMENTAL SECTION

**2.1. Materials.** Zirconyl chloride octahydrate ($ZrOCl_2 \cdot 8H_2O$, 98%, Co., Ltd., ALADDIN Reagent, Shanghai, China, AR), phenylphosphonic acid ($C_6H_7O_3P$, 98%, Sigma−Aldrich), hydrofluoric acid (HF, ≥ 40.0%, ALADDIN Reagent, Shanghai, China, AR), ethanol ($C_2H_6O$, 99.5%, Tianjin kermel Chemical Research Agent Institute, AR), hydrochloric acid (HCl, 36.0−38.0 wt %, Co., Ltd., Shanghai, China, AR) were used as received without further purification.

**2.2. Preparation of ZrPP Powders.** $ZrOCl_2 \cdot 8H_2O$( 0.485 g) and $C_6H_7O_3P$ (0.475 g) were dissolved in a solution containing 15 mL of DI water and 0.45 g of HF with stirring to form a colloidal solution. The mixture was then transferred to a 30 mL Teflon-lined stainless vessel, sealed and put in a rotating oven preheated to 200 °C. After 24 h, the vessel was taken out and cooled to room temperature. Obtained white powders were washed with DI water three times and then dried at 70 °C overnight.

**2.3. Preparation of Zr-Based Sol.** Five grams of $ZrOCl_2 \cdot 8H_2O$ was dissolved in 25 mL of ethanol and vigorously stirred at room temperature for 5 h to obtain a homogeneous white suspension. To avoid precipitation, we added concentrated HCl into the solution dropwise to adjust the pH of the solution to 2.0. The mixture was stirred sequentially for several hours until a clear solution was obtained and then aged for 24 h to obtain the Zr-based sol, which was transparent and remained stable for several months.

**2.4. Preparation of $t$-$ZrO_2$ Buffer Layer.** The $\alpha$-$Al_2O_3$ plate (Fraunhofer IKTS, Germany) with a diameter of 18 mm, thickness of 1 mm, and pore size of 70 nm was fixed on a spin coater. Prepared sol was then rapidly added dropwise and spread over the substrate. Spin-coating was conducted with rotation rate of 3000 rpm for 1.5 min. Finally, the substrate was dried at 70 °C overnight followed by calcination at 400 °C for 4 h with a heating rate of 1 °C $min^{-1}$, which led to the formation of $t$-$ZrO_2$ buffer layer.

**2.5. Preparation of ZrPP Membrane with a Single Zr Source.** Twelve hundredths of a gram of $C_6H_7O_3P$ was dissolved in a solution containing 15 mL of DI water and 0.057 g of hydrofluoric acid with stirring. Subsequently, the $t$-$ZrO_2$ buffer layer-coated $\alpha$-$Al_2O_3$ substrate was vertically placed into a 30 mL Teflon-lined stainless vessel. The mixture was then transferred to the vessel, sealed and put in a convective oven preheated to 100 °C. After 24 h, the vessel was taken out and cooled to room temperature. Finally, the membrane was taken out, washed with copious amounts of DI water, and dried at 70 °C overnight.

**2.6. Preparation of ZrPP Membrane with a Double Zr Source.** $ZrOCl_2 \cdot 8H_2O$ (0.194 g) and $C_6H_7O_3P$ (0.190 g) were dissolved in a solution containing 15 mL of DI water and 0.057 g of hydrofluoric acid with stirring. Subsequently, the $t$-$ZrO_2$ buffer layer-coated $\alpha$-$Al_2O_3$ substrate was vertically placed into a 30 mL Teflon-lined stainless vessel. The mixture was then transferred to the vessel, sealed, and put in a convective oven preheated to 100 °C. After 24 h, the vessel was taken out and cooled to room temperature. Finally, the membrane was taken out, washed with copious amounts of DI water, and dried at 70 °C overnight.

**2.7. Characterizations.** Powder X-ray diffraction (XRD) patterns were recorded in the 2$\theta$ range of 3 and 50° on a Rigaku SmartLab diffractometer with Cu Ka radiation ($\lambda$ = 0.15418 nm) at 45 kV and 200 mA. Morphology of prepared samples was characterized with a Field-emission scanning electron microscope (NOVA NanoSEM 450) operating at 3 keV, work distance (WD) 5 mm, spot size 3.0 and a FlexSEM 1000 SEM operating at 10 keV, work distance (WD) 5 mm, spot size 40. Energy-dispersive X-ray spectrometry (EDX) line

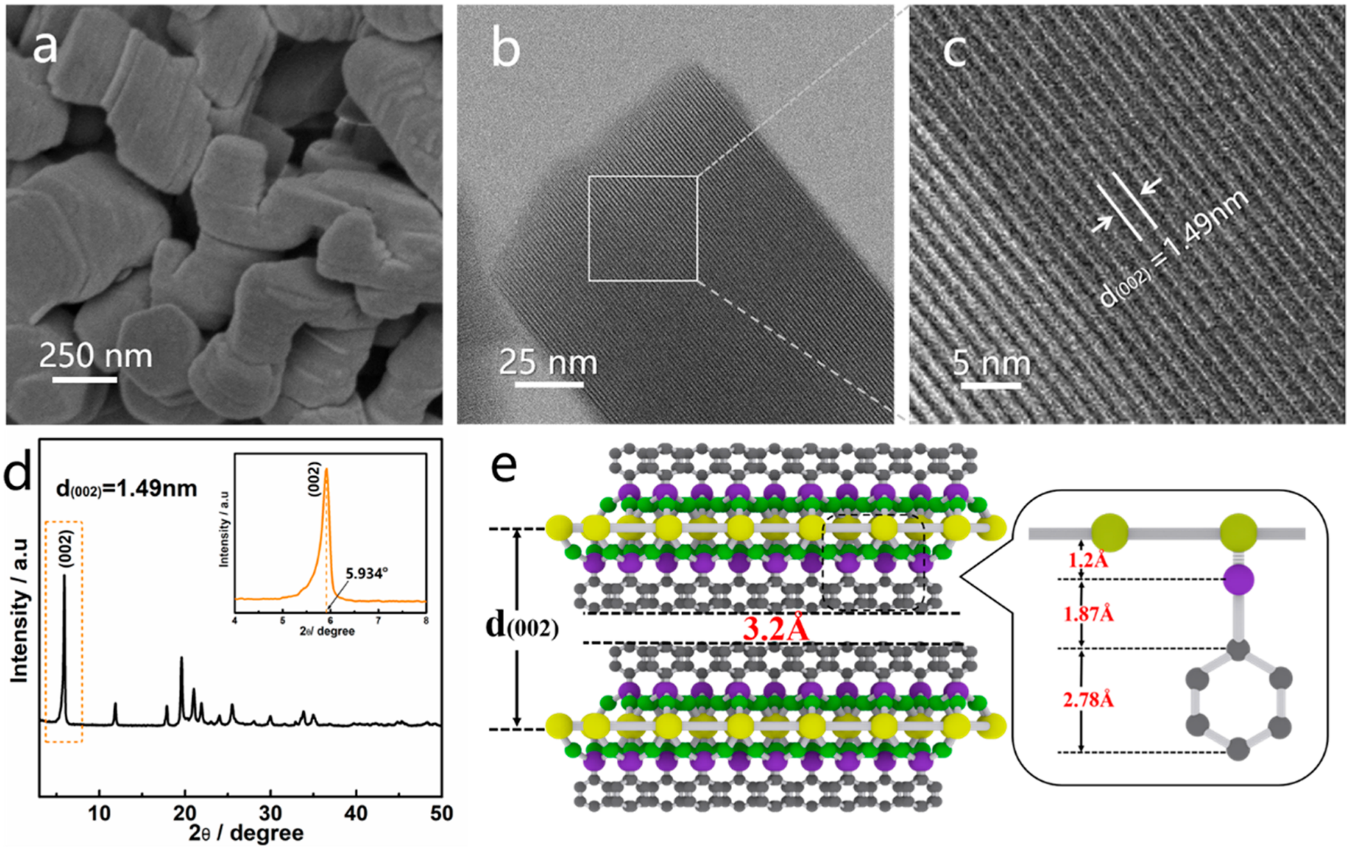

**Figure 2.** (a) SEM image, (b, c) HRTEM images, (d) XRD patterns, and (e) structure illustration of ZrPP crystals.

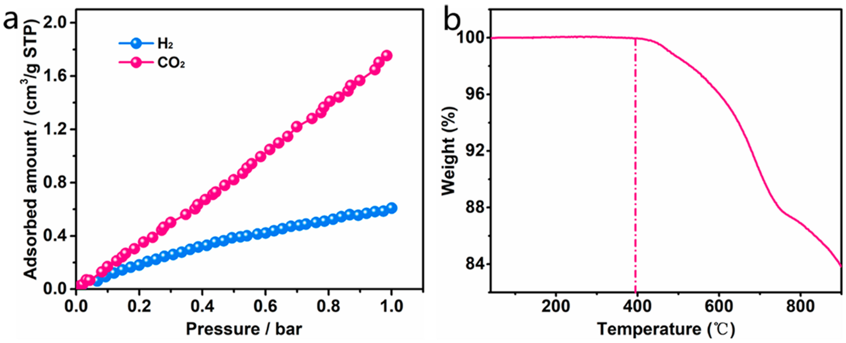

**Figure 3.** (a) Adsorption isotherms of $CO_2$ and $H_2$ on ZrPP powders at 25 °C; (b) TGA curve of ZrPP powders.

scanning analyses were operated with 20 keV of acceleration and 10 mm of working distance. High-resolution transmission electron microscopy (HRTEM) characterization of the microstructure was carried out on a JEM-ARM300F(JEOL) operated at 200 kV. Thermogravimetric analysis (TGA) were carried out under $N_2$ atmosphere with a NETZSCH (TG 209) thermal analyzer at a heating rate of 10 °C/min. Adsorption isotherms were carried out at 25 °C with a micromeritics (ASAP 2020 PLUS HD88).

**2.8. Gas Permeation Test.** Prepared ZrPP membrane was fixed in a module sealed with O-rings. The feed flow rate was kept constant with a volumetric flow rate of 50 mL·min$^{-1}$ for each gas, and permeated gas was removed by sweep gas. Ar was used as the sweep gas with a volumetric flow rate of 50 mL min$^{-1}$. Pressures at both feed and permeate sides were kept at 1 bar. A calibrated gas chromatograph (7890B GC, Agilent) was employed to measure the concentration of mixed gases on the permeate side. The separation factor $\alpha_{i/j}$ of gas pairs is defined as the quotient of the molar ratios of the components ($i$, $j$) in the permeate side, divided by the quotient of the molar ratio of the components ($i$, $j$) in the feed side:

$$\alpha_{i/j} = \frac{X_{i,\text{perm}}/X_{j,\text{perm}}}{X_{i,\text{feed}}/X_{j,\text{feed}}}$$

## 3. RESULTS AND DISCUSSION

### 3.1. Preparation and Characterization of ZrPP Crystals.

Aiming at evaluating their potential in membrane-based separation, we herein investigated structural and physicochemical properties of ZrPP crystals, which were synthesized according to a well-established procedure, prior to the membrane fabrication. As shown in Figure 2a, ZrPP crystals, which were formed by oriented stacking of hexagonal-shaped ZrPP nanoplates with an average grain size around 250 nm (shown in Supporting Infromation SI-3) along the $c$-axis, exhibited a distorted hexagonal-prism-like morphology. HRTEM results (shown in Figure 2b, c and Figure S5) further revealed the uniform spacing of the (002) lattice planes

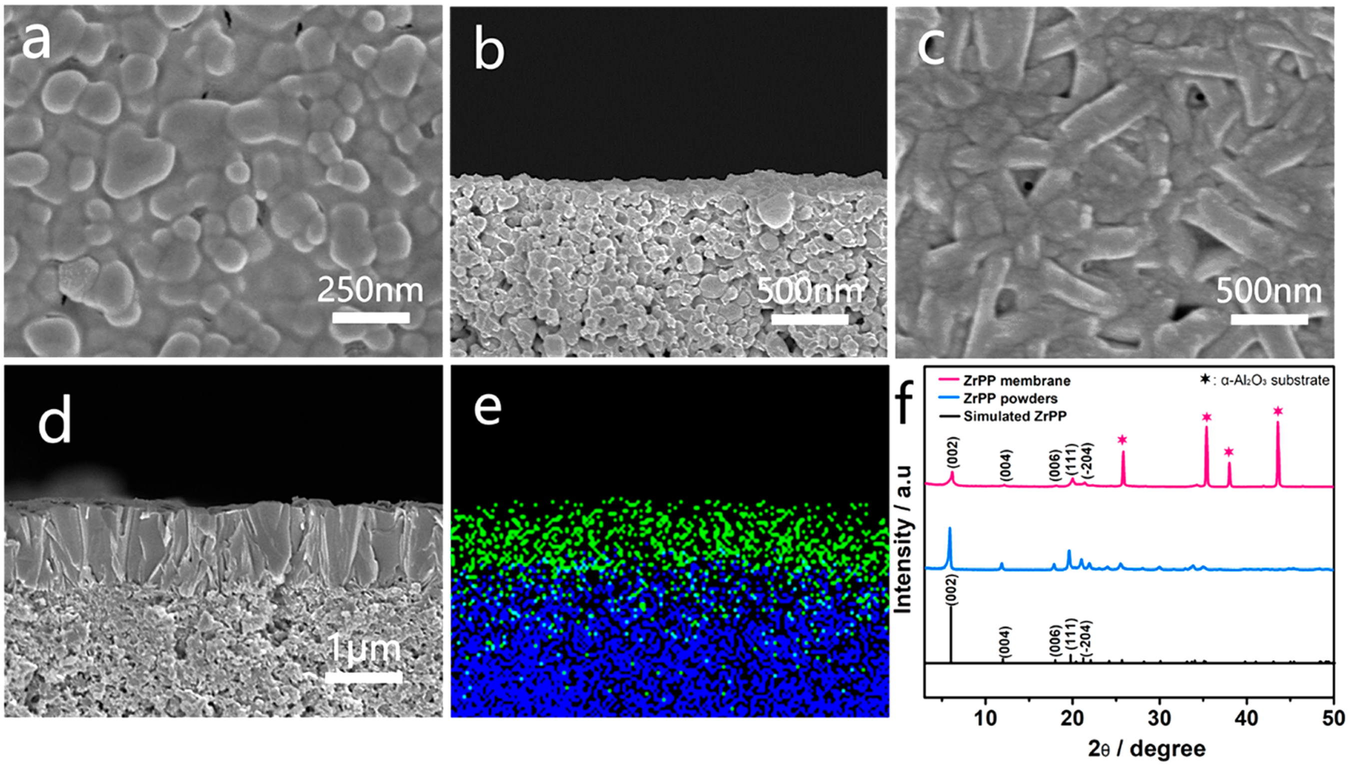

**Figure 4.** SEM images of (a) top and (b) cross-sectional views of the Zr-based layer; (c) top and (d) cross-sectional views of the ZrPP membrane; (e) EDXS mappings of Zr and Al distributions at the cross-section of prepared ZrPP membrane; (f) XRD patterns of simulated ZrPP, ZrPP powders, and prepared ZrPP membrane.

(14.9 Å), which was in good agreement with the basal spacing calculated from the (002) diffraction peak of the XRD pattern (PDF#44−2000) via the Bragg's equation (shown in Figure 2d). The gallery height, which could be obtained by subtracting twice the size of phosphonate functional groups (5.85 Å),[35] was calculated to be 3.2 Å (shown in Figure 2e). This value was smaller than kinetic diameters of most gas molecules except hydrogen (2.9 Å). Combining with the preferential adsorption of $CO_2$ in the framework (Figure 3a) and the extraordinary thermal stability (Figure 3b), ZrPP materials have been considered as promising candidates for high-performance $H_2/CO_2$ selective membranes.

### 3.2. Preparation and Characterization of ZrPP Membranes.

Initially we attempted to prepare well-intergrown ZrPP membranes on bare porous $\alpha$-$Al_2O_3$ substrates by facile in situ hydrothermal growth due to its simplicity. Nevertheless, it turned out to be very difficult to achieve this objective, because of the low-affinity interactions between ZrPP grains and the substrate surface (shown in Supporting Information SI-5). To solve the above problem, we deposited $ZrO_2$ buffer layers, which may also serve as the zirconium source of the ZrPP membrane, on the surface of porous $\alpha$-$Al_2O_3$ substrates prior to hydrothermal synthesis.[38] Spin-coating was found to be very effective in producing uniform precursors of $ZrO_2$ buffer layers. After calcination at 400 °C, zirconia precursor coatings had been fully converted to $ZrO_2$ buffer layers with no obvious cracks or pinholes (shown in Figure 4a, b). XRD patterns of buffer layers after calcination confirmed that formed buffer layers indeed belonged to *t*-$ZrO_2$ phase (shown in Figure S7b). Cross-sectional EDXS results further demonstrated that *t*-$ZrO_2$ buffer layers had partially infiltrated into substrate pores (shown in Supporting Information SI-7). In addition, other zirconia phases could also be obtained under different calcination temperatures. However, they were not as competent as the *t*-$ZrO_2$ phase in terms of the continuity of ZrPP membranes, probably because of the discrepancy in reactivity (shown in Supporting Information SI-6).

The next step refers to hydrothermal conversion of *t*-$ZrO_2$ buffer layers to ZrPP membranes. Initially, a "double zirconium source" concept, i.e., $Zr^{4+}$ ions were provided by both *t*-$ZrO_2$ buffer layers and $ZrOCl_2$ reagents in the precursor solution, was employed. However, our results indicated that ZrPP crystals were only loosely packed on the substrate surface and substantial grain boundary defects existed (shown in Supporting Information SI-8), which could be attributed to preferential nucleation and growth of ZrPP crystals in the bulk solution, resulting in low nucleation density of ZrPP crystals on porous $\alpha$-$Al_2O_3$ substrates. To avoid above-mentioned issue, alternatively, only *t*-$ZrO_2$ buffer layers were served as the zirconium source. Under optimized conditions ([HF] = 0.075 M, $[C_6H_7O_3P]$ = 0.05 M and $T$ = 100 °C, shown in Supporting Information SI-9), *t*-$ZrO_2$ buffer layers were progressively dissolved in the precursor solution as our complementary experiment indicated that *t*-$ZrO_2$ buffer layers were vulnerable to aqueous HF solution corrosion under hydrothermal conditions (shown in Supporting Information SI-10). Because the concentration of nutrients located at the substrate−solution interface was the highest, ZrPP crystals preferentially nucleated on the substrate surface rather than in bulk solution, which ultimately led to the formation of well-intergrown ZrPP membranes.

It was noted that the addition of trace amount of HF, which served as corrosion agents in the precursor solution, was

https://dx.doi.org/10.1021/acsami.0c02789
ACS Appl. Mater. Interfaces 2020, 12, 15320−15327

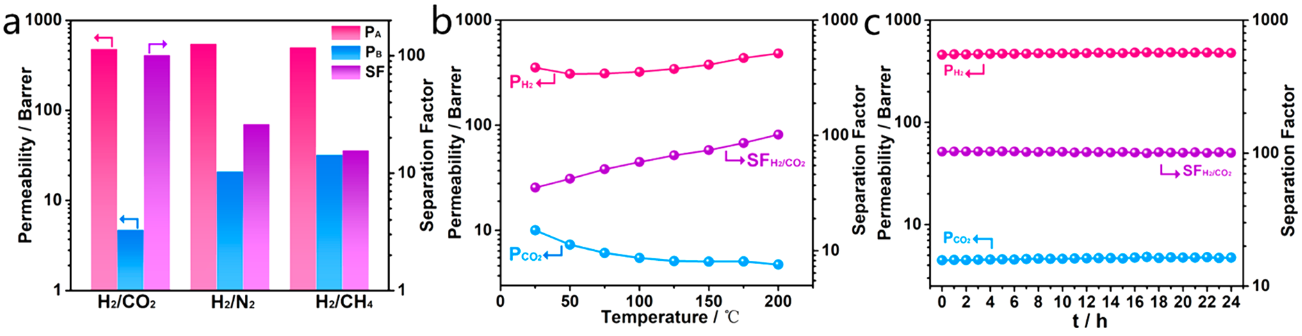

**Figure 5.** (a) Permeability and separation factor of equimolecular $H_2/CO_2$, $H_2/N_2$, and $H_2/CH_4$ mixtures through prepared ZrPP membranes at 200 °C and 1 bar. (b) $H_2$ permeability, $CO_2$ permeability, and SF of mixed $H_2/CO_2$ gas pair on prepared ZrPP membrane as a function of operation temperature. (c) Long-term stability of equimolar $H_2/CO_2$ separation performance of ZrPP membrane at 200 °C and 1 bar with a volumetric flow rate of 50 mL $min^{-1}$ for each gas.

indispensable for the successful conversion of *t*-$ZrO_2$ buffer layers to qualified ZrPP membranes. In the absence of HF, almost no activated $Zr^{4+}$ ions were released from *t*-$ZrO_2$ buffer layers so that ZrPP crystals were only sparsely distributed on substrates; moreover, [HF] in the precursor solution was found to exert significant influence on the microstructure of ZrPP membranes. Maintaining [HF] at 0.075 M led to the formation of ZrPP membranes with optimized microstructure, whereas further increasing [HF] resulted in scattered distribution of ZrPP crystals on porous $\alpha$-$Al_2O_3$ substrates (shown in Figure S10), which was ascribed to the excessive release of $Zr^{4+}$ ions from *t*-$ZrO_2$ buffer layers. In addition, reaction temperature and [$C_6H_7O_3P$] also exerted great influence on the membrane microstructure. For instance, lower reaction temperature led to the formation of ZrPP membranes with obvious gaps along the grain boundary, whereas higher reaction temperatures induced partial detachment of ZrPP crystals from the substrate surface (shown in Figure S11). In addition, increasing [$C_6H_7O_3P$] led to the formation of ZrPP membranes with better intergrowth; nevertheless, the grain size was gradually reduced (shown in Figure S12). Therefore, the reaction condition should be precisely controlled.

As shown in Figure 4c, ZrPP membranes prepared under optimized hydrothermal conditions were well intergrown with the thickness of 1.0 $\mu$m (shown in Figure 4d). Cross-sectional EDXS patterns (shown in Figure 4e) further indicated that ZrPP membranes had partially penetrated substrate pores, which was very beneficial for enhancing their mechanical stability. XRD patterns (shown in Figure 4f) further confirmed that prepared membranes indeed belonged to pure ZrPP phase due to the appearance of clearly distinguishable diffraction peaks at 2$\theta$ values of 5.9, 19.7, and 21.1° corresponding to (002), (111) and (−204) crystal planes of ZrPP powders. It should be emphasized that although the preferred orientation of prepared ZrPP membrane could not be directly identified according to the XRD pattern due to partial penetration of ZrPP membranes into the substrate pores, both top and cross-sectional SEM images clearly revealed that most ZrPP crystals should be vertically aligned on the substrate surface due to "evolution selection", a principle proposed by Van der Drift in interpretation of the preferred orientation of a vapor-deposited PbO layer,[39,40] which could be further evidenced by a recent study on in situ crystallization of highly oriented ZrPP films on Cu substrates under similar hydrothermal conditions.[26] Vertical alignment of ZrPP crystals should be, in principle, very advantageous for improving their separation performance as mentioned above.

**3.3. Separation Performance and Durability of ZrPP Membranes.** To quantitatively evaluate their gas separation performance, we measured volumetric flow rates of different binary gas mixtures through prepared ZrPP membranes at 200 °C and 1 bar (shown in Figure 5a). It was observed that the separation factor (SF) for equimolecular $H_2/CO_2$, $H_2/N_2$, and $H_2/CH_4$ gas pairs reached 101.2, 26.2, and 15.7, respectively, which were well above their Knudsen selectivity (4.7, 3.7, and 2.8) indicating that the gas permeation behavior was dominated by a size-exclusion mechanism. Particularly, the separation performance of ZrPP membranes toward $H_2/CO_2$ mixtures not only easily exceeded the 2008 Robeson upper-bound line[41] but also was superior to other reported Zr-based MOF membranes (shown in Figure 6).[42−44] A much lower permeability of $CO_2$ in comparison with $N_2$ and $CH_4$ indicated strong interactions between $CO_2$ and polarized ZrPP framework,[33] leading to significantly reduced diffusion coefficient of $CO_2$. Simultaneously, the preferential adsorption toward $CO_2$ was also illustrated by $CO_2$ adsorption isotherms on ZrPP powders (shown in Figure 3a).

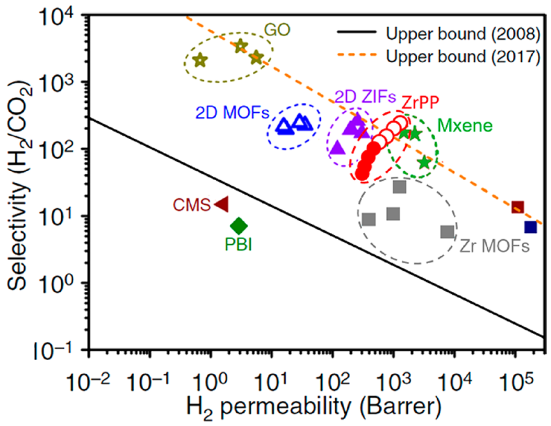

**Figure 6.** Comparison of the experimental (red closed circle) and extrapolated (red open circle) $H_2/CO_2$ separation performance of prepared ZrPP membranes at different temperature (the temperature from the bottom to the top corresponds to 50, 100, 150, 200, 250, 300, 350, and 400 °C, respectively).

The effect of operating temperature on the separation performance of $H_2/CO_2$ gas pair was further investigated (shown in Figure 5b). It was observed that both $H_2$ permeability and $H_2/CO_2$ SF steadily increased in case the temperature increased from 50 to 200 °C, which could be attributed to a gradual pronounced size-exclusion mechanism with increasing temperature. Although the separation performance above 200 °C could not be measured due to the upper operating temperature limit of the permeation cell, the separation performance of ZrPP membranes at higher temperatures could be reasonably predicated by extrapolating existing $H_2/CO_2$ SF and $H_2$ permeability data as a function of operating temperature (shown in Supporting Information SI-11). It was exciting to note that SF of $H_2/CO_2$ of prepared ZrPP membranes at 350 and 400 °C obtained by fitting existing experimental data readily exceeded the 2017 upper bound line (shown in Figure 6).[45] Despite the need for further experimental validation, our supplementary experiment indicated that both ZrPP powders and membranes were thermally stable up to 400 °C without substantial weight loss, morphological damage or structural degradation (shown in Figure 3b and Figure S15). Further experimental validation of the actual $H_2/CO_2$ separation performance of ZrPP membranes at higher temperature should be conducted in the future.

Finally, to evaluate the durability of ZrPP membranes under harsh operating conditions, their thermal, mechanical, and chemical stability was further measured. First, the long-term thermal stability was evaluated. It was noted that LDH membranes could not withstand operating temperature above 180 °C because of an irreversible collapse of the layered structure.[23,24,46] In contrast, ZrPP membranes could withstand higher operating temperature. For instance, our results indicated that both $H_2$ permeability and SF of equimolar $H_2/CO_2$ gas pair remained constant within 24 h at 200 °C and 1 bar with a volumetric flow rate of 50 $\text{mL}\cdot\text{min}^{-1}$ for each gas (shown in Figure 5c). Second, their mechanical stability was evaluated by sonication in distilled water for 1 h. After sonication, prepared membranes remained firmly attached to porous $\alpha$-$Al_2O_3$ substrates (shown in Supporting Information SI-13). Third, their chemical stability was evaluated by immersing in aqueous solutions with different pH values. It was observed that both crystal structure and surface morphology of ZrPP membranes remained intact within a broad pH range (1−12) for 24 h at room temperature (shown in Supporting Information SI-14). Extraordinary thermal, mechanical and chemical stability rendered ZrPP membranes potentially attractive for long-term operation (like recovery of $CO_2$ from the power plants and flue gases at high temperature) under harsh operating conditions. Combining with the gallery height tunability and functional diversity,[34−36] it is believed that a wide variety of zirconium phosphates are attractive candidates for membrane-based separation applications.

## 4. CONCLUSIONS

To summarize, in this study, well-intergrown ZrPP membranes with vertically aligned interlayer galleries were prepared on porous $\alpha$-$Al_2O_3$ substrates by facile in situ hydrothermal growth. Surface modification of the substrate with *t*-$ZrO_2$ buffer layers led to the formation of well-intergrown and oriented ZrPP membranes. Adding trace amount of HF played a key role in balancing the dissolution rate of *t*-$ZrO_2$ buffer layers and growth rate of ZrPP membranes. ZrPP membranes prepared under optimized synthetic conditions exhibited excellent $H_2/CO_2$ separation performance (SF > 100) due to an appropriate interlayer height (3.2 Å) as well as strong interactions between $CO_2$ and polarized ZrPP framework. In addition, prepared ZrPP membranes exhibited exceptional thermal, chemical, and mechanical stability, making them superb candidates for efficient $H_2/CO_2$ separation.

## ASSOCIATED CONTENT

### Supporting Information

The Supporting Information is available free of charge at https://pubs.acs.org/doi/10.1021/acsami.0c02789.

> Structure illustration of ZrPP crystals; effect of crystallization time on morphology and crystallinity of ZrPP powders; morphology and size distribution of ZrPP crystals; HRTEM calibration profile of ZrPP crystals; SEM image of ZrPP membrane prepared by in situ hydrothermal growth; information on Zr-based sol, $ZrO_2$ buffer layers and related ZrPP membranes; cross-sectional SEM image and EDXS pattern of *t*-$ZrO_2$ buffer layer; SEM images of ZrPP membrane prepared with “double zirconium source” method; optimization of synthetic conditions of ZrPP membranes prepared with single Zr source; stability of the *t*-$ZrO_2$ buffer layers in HF solution; experimental and extrapolated $H_2/CO_2$ separation performance of prepared ZrPP membrane at different operation temperature; investigation of the thermal, mechanical, and chemical stability of ZrPP membrane (PDF)

## AUTHOR INFORMATION

### Corresponding Author

**Yi Liu** − *State Key Laboratory of Fine Chemicals, School of Chemical Engineering, Dalian University of Technology, Dalian 116024, China*; Email: diligenliu@dlut.edu.cn

### Authors

**Taotao Ji** − *State Key Laboratory of Fine Chemicals, School of Chemical Engineering, Dalian University of Technology, Dalian 116024, China*

**Yanwei Sun** − *State Key Laboratory of Fine Chemicals, School of Chemical Engineering, Dalian University of Technology, Dalian 116024, China*

**Yi Liu** − *State Key Laboratory of Fine Chemicals, School of Chemical Engineering, Dalian University of Technology, Dalian 116024, China*

**Mingrun Li** − *State Key Laboratory of Catalysis, Dalian Institute of Chemical Physics, Chinese Academy of Sciences, Dalian 116024, China*

**Fei Wang** − *State Key Laboratory of Structural Chemistry, Fujian Institute of Research on the Structure of Matter, Chinese Academy of Sciences, Fuzhou 350002, China*; orcid.org/0000-0001-8432-0009

**Liangliang Liu** − *State Key Laboratory of Fine Chemicals, School of Chemical Engineering, Dalian University of Technology, Dalian 116024, China*

**Gaohong He** − *State Key Laboratory of Fine Chemicals, School of Chemical Engineering, Dalian University of Technology, Dalian 116024, China*; orcid.org/0000-0002-6674-8279

Complete contact information is available at: https://pubs.acs.org/10.1021/acsami.0c02789

### Author Contributions

The manuscript was written through contributions of all authors. All authors have given approval to the final version of the manuscript.

### Notes

The authors declare no competing financial interest.

## ■ ACKNOWLEDGMENTS

The authors are grateful to National Natural Science Foundation of China (21176231), Liaoning Revitalization Talents Program (XLYC1807084), the Thousand Youth Talents Program, and the Technology Innovation Team of Dalian University of Technology (DUT2017TB01) for the financial support.

## ■ REFERENCES

(1) Kosinov, N.; Gascon, J.; Kapteijn, F.; Hensen, E. J. M. Recent Developments in Zeolite Membranes for Gas Separation. *J. Membr. Sci.* **2016**, *499*, 65−79.

(2) Rangnekar, N.; Mittal, N.; Elyassi, B.; Caro, J.; Tsapatsis, M. Zeolite Membranes: A Review and Comparison with MOFs. *Chem. Soc. Rev.* **2015**, *44*, 7128−7154.

(3) Qiu, S.; Xue, M.; Zhu, G. Metal-organic Framework Membranes: from Synthesis to Separation Application. *Chem. Soc. Rev.* **2014**, *43*, 6116−6140.

(4) Shah, M.; McCarthy, M. C.; Sachdeva, S.; Lee, A. K.; Jeong, H. K. Current Status of Metal−Organic Framework Membranes for Gas Separations: Promises and Challenges. *Ind. Eng. Chem. Res.* **2012**, *51*, 2179−2199.

(5) Jang, K. S.; Kim, H. J.; Johnson, J. R.; Kim, W. g.; Koros, W. J.; Jones, C. W.; Nair, S. Modified Mesoporous Silica Gas Separation Membranes on Polymeric Hollow Fibers. *Chem. Mater.* **2011**, *23*, 3025−3028.

(6) Ma, X.; Swaidan, R.; Teng, B.; Tan, H.; Salinas, O.; Litwiller, E.; Han, Y.; Pinnau, I. Carbon Molecular Sieve Gas Separation Membranes Based on an Intrinsically Microporous Polyimide Precursor. *Carbon* **2013**, *62*, 88−96.

(7) Liu, Y.; Ban, Y.; Yang, W. Microstructural Engineering and Architectural Design of Metal-Organic Framework Membranes. *Adv. Mater.* **2017**, *29*, 1606949.

(8) Knebel, A.; Geppert, B.; Volgmann, K.; Kolokolov, D. I.; Stepanov, A. G.; Twiefel, J.; Heitjans, P.; Volkmer, D.; Caro, J. Defibrillation of Soft Porous Metal-organic Frameworks with Electric Fields. *Science* **2017**, *358*, 347−351.

(9) Xue, D.-X.; Cadiau, A.; Weselinski, Łu. J.; Jiang, H.; Bhatt, P. M.; Shkurenko, A.; Wojtas, L.; Zhijie, C.; Belmabkhout, Y.; Adil, K.; Eddaoudi, M. Topology Meets MOF Chemistry for Pore-aperture Fine Tuning: Ftw-MOF Platform for Energy-efficient Separations via Adsorption Kinetics or Molecular Sieving. *Chem. Commun.* **2018**, *54*, 6404−6407.

(10) Zhou, S.; Wei, Y.; Li, L.; Duan, Y.; Hou, Q.; Zhang, L.; Ding, L. X.; Xue, J.; Wang, H.; Caro, J. Paralyzed Membrane: Current-driven Synthesis of a Metal-organic Framework with Sharpened Propene/propane Separation. *Sci. Adv.* **2018**, *4*, No. eaau1393.

(11) Sun, Y.; Liu, Y.; Caro, J.; Guo, X.; Song, C.; Liu, Y. In-Plane Epitaxial Growth of Highly c-Oriented NH$_2$ -MIL-125(Ti) Membranes with Superior H$_2$ /CO$_2$ Selectivity. *Angew. Chem., Int. Ed.* **2018**, *57*, 16088−16093.

(12) Bux, H.; Feldhoff, A.; Cravillon, J.; Wiebcke, M.; Li, Y. S.; Caro, J. Oriented Zeolitic Imidazolate Framework-8 Membrane with Sharp H$_2$/C$_3$H$_8$ Molecular Sieve Separation. *Chem. Mater.* **2011**, *23*, 2262−2269.

(13) Lai, Z. P.; Tsapatsis, M. Gas and Organic Vapor Permeation Through b-oriented MFI Membranes. *Ind. Eng. Chem. Res.* **2004**, *43*, 3000−3007.

(14) Lai, Z. P.; Bonilla, G.; Diaz, I.; Nery, J. G.; Sujaoti, K.; Amat, M. A.; Kokkoli, E.; Terasaki, O.; Thompson, R. W.; Tsapatsis, M.; Vlachos, D. G. Microstructural Optimization of a Zeolite Membrane for Organic Vapor Separation. *Science* **2003**, *300*, 456−460.

(15) Peng, Y.; Lu, H.; Wang, Z.; Yan, Y. Microstructural Optimization of MFI-type Zeolite Membranes for Ethanol−water Separation. *J. Mater. Chem. A* **2014**, *2*, 16093−16100.

(16) Xia, S.; Peng, Y.; Wang, Z. Microstructure Manipulation of MFI-type Zeolite Membranes on Hollow Fibers for Ethanol−water Separation. *J. Membr. Sci.* **2016**, *498*, 324−335.

(17) Kim, H. W.; Yoon, H. W.; Yoon, S. M.; Yoo, B. M.; Ahn, B. K.; Cho, Y. H.; Shin, H. J.; Yang, H.; Paik, U.; Kwon, S.; Choi, J. Y.; Park, H. B. Selective Gas Transport Through Few-Layered Graphene and Graphene Oxide Membranes. *Science* **2013**, *342*, 91−95.

(18) Shen, J.; Liu, G.; Ji, Y.; Liu, Q.; Cheng, L.; Guan, K.; Zhang, M.; Liu, G.; Xiong, J.; Yang, J.; Jin, W. 2D MXene Nanofilms with Tunable Gas Transport Channels. *Adv. Funct. Mater.* **2018**, *28*, 1801511.

(19) Hirunpinyopas, W.; Prestat, E.; Worrall, S. D.; Haigh, S. J.; Dryfe, R. A. W.; Bissett, M. A. Desalination and Nanofiltration through Functionalized Laminar MoS$_2$ Membranes. *ACS Nano* **2017**, *11*, 11082−11090.

(20) Roth, W. J.; Nachtigall, P.; Morris, R. E.; Cejka, J. Two-Dimensional Zeolites: Current Status and Perspectives. *Chem. Rev.* **2014**, *114*, 4807−4837.

(21) Liu, G.; Jin, W.; Xu, N. Graphene-based Membranes. *Chem. Soc. Rev.* **2015**, *44*, 5016−5030.

(22) Zhao, M.; Huang, Y.; Peng, Y.; Huang, Z.; Ma, Q.; Zhang, H. Two-dimensional Metal-organic Framework Nanosheets: Synthesis and Applications. *Chem. Soc. Rev.* **2018**, *47*, 6267−6295.

(23) Liu, Y.; Wang, N.; Caro, J. In Situ Formation of LDH Membranes of Different Microstructures with Molecular Sieve Gas Selectivity. *J. Mater. Chem. A* **2014**, *2*, 5716−5723.

(24) Liu, Y.; Wang, N.; Cao, Z.; Caro, J. Molecular Sieving through Interlayer Galleries. *J. Mater. Chem. A* **2014**, *2*, 1235−1238.

(25) Wang, Z.; Heising, J. M.; Clearfield, A. Sulfonated Microporous Organic-inorganic Hybrids as Strong Bronsted acids. *J. Am. Chem. Soc.* **2003**, *125*, 10375−10383.

(26) Cui, Z.; Zhang, F.; Wang, L.; Xu, S.; Guo, X. In Situ Crystallized Zirconium Phenylphosphonate Films with Crystals Vertically to the Substrate and Their Hydrophobic, Dielectric, and Anticorrosion Properties. *Langmuir* **2010**, *26*, 179−182.

(27) Diaz, A.; Saxena, V.; Gonzalez, J.; David, A.; Casanas, B.; Carpenter, C.; Batteas, J. D.; Colon, J. L.; Clearfield, A.; Delwar Hussain, M. Zirconium Phosphate Nano-platelets: A Novel Platform for Drug Delivery in Cancer Therapy. *Chem. Commun.* **2012**, *48*, 1754−1756.

(28) Pica, M.; Nocchetti, M.; Ridolfi, B.; Donnadio, A.; Costantino, F.; Gentili, P. L.; Casciola, M. Nanosized Zirconium Phosphate/AgCl Composite Materials: A New Synergy for Efficient Photocatalytic Degradation of Organic Dye Pollutants. *J. Mater. Chem. A* **2015**, *3*, 5525−5534.

(29) Mu, W.; Yu, Q.; Zhang, R.; Li, X.; Hu, R.; He, Y.; Wei, H.; Jian, Y.; Yang, Y. Controlled Fabrication of Flower-like-zirconium Phosphate for the Efficient Removal of Radioactive Strontium from Acidic Nuclear Wastewater. *J. Mater. Chem. A* **2017**, *5*, 24388−24395.

(30) Cavka, J. H.; Jakobsen, S.; Olsbye, U.; Guillou, N.; Lamberti, C.; Bordiga, S.; Lillerud, K. P. A New Zirconium Inorganic Building Brick Forming Metal Organic Frameworks with Exceptional Stability. *J. Am. Chem. Soc.* **2008**, *130*, 13850−13851.

(31) Kandiah, M.; Nilsen, M. H.; Usseglio, S.; Jakobsen, S.; Olsbye, U.; Tilset, M.; Larabi, C.; Quadrelli, E. A.; Bonino, F.; Lillerud, K. P. Synthesis and Stability of Tagged UiO-66 Zr-MOFs. *Chem. Mater.* **2010**, *22*, 6632−6640.

(32) Liu, X.; Demir, N. K.; Wu, Z.; Li, K. Highly Water-Stable Zirconium Metal Organic Framework UiO-66 Membranes Supported on Alumina Hollow Fibers for Desalination. *J. Am. Chem. Soc.* **2015**, *137*, 6999−7002.

(33) Unnikrishnan, P.; Varhadi, P.; Srinivas, D. Efficient, Direct Synthesis of Dimethyl Carbonate from CO$_2$ Using a Solid, Calcined

Zirconium Phenylphosphonate Phosphite Catalyst. *RSC Adv.* **2013**, *3*, 23993−23996.

(34) Clearfield, A.; Wang, Z. Organically Pillared Microporous Zirconium Phosphonates. *J. Chem. Soc., Dalton Trans.* **2002**, 2937−2947.

(35) Alberti, G.; Costantino, U.; Allulli, S.; Tomassini, N. Crystalline $Zr(R\text{-}PO_3)_2$ AND $Zr(R\text{-}OPO_3)_2$ Compounds (R = Organic Radical) - New Class of Materials Having Layered Structure of Zirconium-Phosphate Type. *J. Inorg. Nucl. Chem.* **1978**, *40*, 1113−1117.

(36) Poojary, M. D.; Hu, H. L.; Campbell, F. L.; Clearfield, A. Determination of Crystal-Structures from Limited Powder Data Sets - Crystal-Structure of Zirconium Phenylphosphonate. *Acta Crystallogr., Sect. B: Struct. Sci.* **1993**, *49*, 996−1001.

(37) Qiao, Z.; Zhao, S.; Wang, J.; Wang, S.; Wang, Z.; Guiver, M. D. A Highly Permeable Aligned Montmorillonite Mixed-Matrix Membrane for $CO_2$ Separation. *Angew. Chem., Int. Ed.* **2016**, *55*, 9321−9325.

(38) Wu, F.; Cao, Y.; Liu, H.; Zhang, X. High-performance UiO-66-$NH_2$ Tubular Membranes by Zirconia-induced Synthesis for Desulfurization of Model Gasoline via Pervaporation. *J. Membr. Sci.* **2018**, *556*, 54−65.

(39) Van Der Drift, A. Evolutionary Selection, a Principle Governing Growth Orientation in Vapour-deposited Layers. *Philips Res. Rep.* **1967**, *22*, 267−288.

(40) Li, Y. S.; Bux, H.; Feldhoff, A.; Li, G. L.; Yang, W. S.; Caro, J. Controllable Synthesis of Metal-organic Frameworks: From MOF Nanorods to Oriented MOF Membranes. *Adv. Mater.* **2010**, *22*, 3322−3326.

(41) Robeson, L. M. The Upper Bound Revisited. *J. Membr. Sci.* **2008**, *320*, 390−400.

(42) Sun, Y.; Song, C.; Guo, X.; Liu, Y. Concurrent Manipulation of Out-of-Plane and Regional In-Plane Orientations of $NH_2$-UiO-66 Membranes with Significantly Reduced Anisotropic Grain Boundary and Superior $H_2/CO_2$ Separation Performance. *ACS Appl. Mater. Interfaces* **2020**, *12*, 4494−4500.

(43) Friebe, S.; Geppert, B.; Steinbach, F.; Caro, J. Metal-Organic Framework UiO-66 Layer: A Highly Oriented Membrane with Good Selectivity and Hydrogen Permeance. *ACS Appl. Mater. Interfaces* **2017**, *9*, 12878−12885.

(44) Knebel, A.; Sundermann, L.; Mohmeyer, A.; Strauß, I.; Friebe, S.; Behrens, P.; Caro, J. Azobenzene Guest Molecules as Light-Switchable $CO_2$ Valves in an Ultrathin UiO-67 Membrane. *Chem. Mater.* **2017**, *29*, 3111−3117.

(45) Ding, L.; Wei, Y.; Li, L.; Zhang, T.; Wang, H.; Xue, J.; Ding, L. X.; Wang, S.; Caro, J.; Gogotsi, Y. MXene Molecular Sieving Membranes for Highly Efficient Gas Separation. *Nat. Commun.* **2018**, *9*, 155.

(46) Wang, Q.; O'Hare, D. Recent Advances in the Synthesis and Application of Layered Double Hydroxide (LDH) Nanosheets. *Chem. Rev.* **2012**, *112*, 4124−4155.